

UNCLASSIFIED

AD 635 185

DETERMINATION OF WINDS FROM METEOROLOGICAL
ROCKETSONDES

Amos Eddy, et al

The University of Texas
Austin, Texas

November 1965

Processed for . . .

DEFENSE DOCUMENTATION CENTER
DEFENSE SUPPLY AGENCY



U. S. DEPARTMENT OF COMMERCE / NATIONAL BUREAU OF STANDARDS / INSTITUTE FOR APPLIED TECHNOLOGY

UNCLASSIFIED

AD 635185

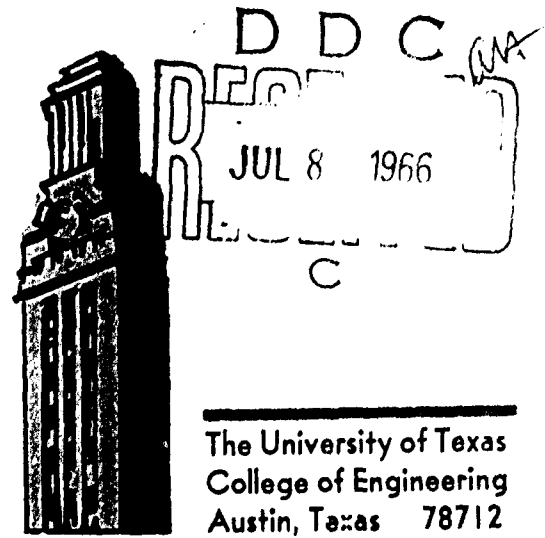
DETERMINATION OF WINDS FROM METEOROLOGICAL
ROCKETSONDES

Eddy, Duchon, Haase, and Haragan

Report No. 2

November 1965

CLEARINGHOUSE FOR FEDERAL SCIENTIFIC AND TECHNICAL INFORMATION			
Hardcopy	Microfiche		
\$ 2.00	\$.50	34 pp	as
1 ARCHIVE COPY			



**ATMOSPHERIC
SCIENCE GROUP**

The University of Texas
College of Engineering
Austin, Texas 78712

Reproduced by the
CLEARINGHOUSE
for Federal Scientific & Technical
Information Springfield Va. 22151

A

ACCESSION for		
CFSTI	WHITE SECTION	<input checked="" type="checkbox"/>
ODC	DIFF SECTION	<input type="checkbox"/>
UNANNOUNCED		<input type="checkbox"/>
JUSTIFICATION		
BY		
DISTRIBUTION/AVAILABILITY CODE		
DIST.	AVAIL.	and/or SPECIAL
1		

ATMOSPHERIC SCIENCE GROUP
College of Engineering
The University of Texas
Austin, Texas

Report No. 2

November 1965

DETERMINATION OF WINDS FROM METEOROLOGICAL ROCKETSONDES

Amos Eddy
C. M. Duchon
F. A. Haase
D. E. Haragan

Sponsored by

U. S. Army Electronics Research and Development Activity
Environmental Sciences Department, White Sands Missile Range
under Contract DA-23-072-AMC-1564

ABSTRACT

The equations of motion are derived for an object falling under the influence of gravity and aerodynamic drag. These equations are used to examine the response of the ARCAS parachute to hypothetical wind profiles in the region extending from 30 to 80 km.

A computational scheme for determining the horizontal wind from the observed motion of any wind sensor influenced only by the above forces is presented, along with an example of its application to an ARCAS parachute flight.

TABLE OF CONTENTS

	Page
ABSTRACT	ii
LIST OF FIGURES	iv
1. INTRODUCTION	1
2. EQUATIONS OF MOTION	1
3. QUALITATIVE RESPONSE CHARACTERISTICS	6
4. QUANTITATIVE RESPONSE CHARACTERISTICS	7
5. APPLICATION TO REAL WIND DATA	20
6. SUMMARY	27
REFERENCES	29

LIST OF FIGURES

No.		Page
1	Combination force and velocity vector diagram applied to a wind sensor of mass m with velocity \vec{V}_p in a wind field with velocity \vec{V} and acting under the influence of gravity $m\vec{g}$ and drag force \vec{D}	3
2	Response of sensor speed U_p to oscillatory wind speed U of amplitude A_m and wavelength L under steady-state conditions. ψ is the phase angle.	8
3	Scheme of idealized ARCAS parachute flight	10
4	Plot of height vs drag coefficient	12
5	Plot of height vs horizontal speed and fall speed of ARCAS parachute	15
6	Plot of height vs horizontal parachute and wind speeds	17
7	Plot of height vs fall speed	18
8	Plot of height vs horizontal parachute and wind speeds	19
9	Frequency response of ARCAS parachute vs wavelength at various heights	21
10	Height vs phase angle $\psi = \tan^{-1} \frac{2\pi}{KL}$ for various wavelengths	22
11	Frequency response functions	25
12	Response as a function of wavelength for various heights	25
13	Computed wind speeds from observed parachute speeds	26

I. INTRODUCTION

One important question asked by atmospheric scientists involved in the analysis of rocketsonde data concerns the accuracy of the wind information. At present, the wind information available to the analyst (Data Reports of the Meteorological Rocket Network Firings) is determined directly from the motion of the wind sensor without any corrections applied. In addition, the data presentation commonly begins at some height considerably below apogee (the highest point attained by the sensor).

The purpose of this report is twofold:

1. To investigate the response of a wind sensor to its environment.
2. To demonstrate the feasibility of applying corrections to the sensor motion in order to obtain the real wind, and of extending the wind data to higher altitudes.

2. EQUATIONS OF MOTION

We shall assume from the outset that the wind sensor moves only in response to the force of gravity and aerodynamic drag.

From Newton's second law of motion, we can write

$$m \frac{d\vec{v}_p}{dt} = m\vec{g} + \vec{D} \quad (1)$$

where m is the mass of the sensor, $d\vec{v}_p/dt$ the instantaneous sensor acceleration, \vec{g} the acceleration due to gravity (assumed constant) and

\vec{D} the drag force.

Figure 1 is a combination force and velocity vector diagram and illustrates the relationship among the terms in (1) and their relationship to sensor velocity \vec{V}_p and wind velocity \vec{V} . Also shown are the scalar components of $(\vec{V} - \vec{V}_p)$.

The magnitude of the drag force is assumed proportional to the square of the velocity of the air relative to the velocity of the sensor and can be expressed

$$|\vec{D}| = \rho \frac{C_D A}{2} |\vec{V} - \vec{V}_p|^2, \quad (2)$$

where ρ is air density, C_D the drag coefficient, and A a characteristic area of the sensor.

From Fig. 1, the drag force expanded into component form yields

$$\vec{D} = \vec{i} |\vec{D}| \cos \alpha + \vec{j} |\vec{D}| \cos \beta + \vec{k} |\vec{D}| \cos \gamma$$

and, further, as

$$\vec{D} = \vec{i} |\vec{D}| u_r |\vec{V} - \vec{V}_p|^{-1} + \vec{j} |\vec{D}| v_r |\vec{V} - \vec{V}_p|^{-1} + \vec{k} |\vec{D}| w_r |\vec{V} - \vec{V}_p|^{-1} \quad (3)$$

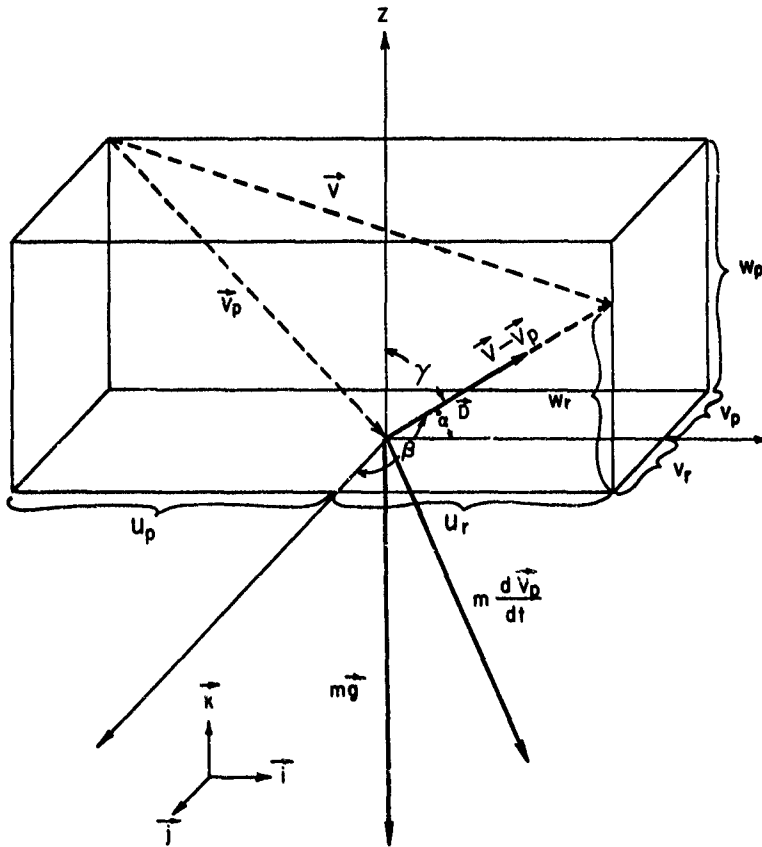
where u_r , v_r , and w_r are the components of air speed relative to the sensor.

Substituting (2) into (3) and recognizing that $|\vec{V} - \vec{V}_p| = [u_r^2 + v_r^2 + w_r^2]^{1/2}$

we obtain

$$\vec{D} = (\vec{i} u_r + \vec{j} v_r + \vec{k} w_r) [u_r^2 + v_r^2 + w_r^2]^{1/2} \rho C_D A / 2. \quad (4)$$

Substituting (4) into (1) and expressing the result in component form, we get



COMBINATION FORCE AND VELOCITY VECTOR DIAGRAM
 APPLIED TO A WIND SENSOR OF MASS m WITH VELOCITY
 \vec{V}_p IN WIND FIELD WITH VELOCITY \vec{V} AND ACTING
 UNDER INFLUENCE OF GRAVITY $m\vec{g}$ AND DRAG FORCE \vec{D}

FIG. 1.

$$\frac{du_p}{dt} = u_r K [u_r^2 + v_r^2 + w_r^2]^{1/2}, \quad (5)$$

$$\frac{dv_p}{dt} = v_r K [u_r^2 + v_r^2 + w_r^2]^{1/2} \quad (6)$$

and

$$\frac{dw_p}{dt} = -g + w_r K [u_r^2 + v_r^2 + w_r^2]^{1/2} \quad (7)$$

where $K = \rho C_D A / 2m$.

It is desirable with respect to the analysis that follows to change the independent variable from time to height. Accordingly, since

$$\frac{du_p}{dt} = \frac{du_p}{dz} \frac{dz}{dt} = w_p \frac{du_p}{dz}$$

and similarly for dv_p/dt and dw_p/dt , the equations of motion can also be written

$$\frac{du_p}{dz} = u_r w_p^{-1} K [u_r^2 + v_r^2 + w_r^2]^{1/2}, \quad (8)$$

$$\frac{dv_p}{dz} = v_r w_p^{-1} K [u_r^2 + v_r^2 + w_r^2]^{1/2}, \quad (9)$$

and

$$\frac{dw_p}{dz} = -g w_p^{-1} + w_r w_p^{-1} K [u_r^2 + v_r^2 + w_r^2]^{1/2}. \quad (10)$$

In the following development we shall assume that the vertical component of the wind, w , is zero. Since, in general, $w_r = w - w_p$ our assumption makes $w_r = -w_p$ and, consequently, the latter set of equations becomes

$$\frac{du_p}{dz} = -u_r K \left[1 + \frac{u_r^2 + v_r^2}{w_p^2} \right]^{1/2} \quad (11)$$

$$\frac{dv_p}{dz} = -v_r K \left[1 + \frac{u_r^2 + v_r^2}{w_p^2} \right]^{1/2} \quad (12)$$

and

$$\frac{dw_p}{dz} = -g w_p^{-1} + w_p K \left[1 + \frac{u_r^2 + v_r^2}{w_p^2} \right]^{1/2}. \quad (13)$$

It is significant to observe that, for the condition of zero vertical wind, the error in the horizontal wind components, u_r and v_r , can be determined from the sensor velocity alone, without regard to the physical characteristics of the medium and sensor that are involved in K . However, since there is no unique sensor velocity profile, this approach in determining u_r and v_r can be utilized in real situations only. An example of employing this approach is reserved for a later section.

In order to permit a more general understanding of how the sensor will respond to its environment, we shall therefore postulate the state of the environment.

3. QUALITATIVE RESPONSE CHARACTERISTICS

Since we have already assumed no vertical wind, our immediate concern is with (11) and (12). Because they are similar, we shall consider only (11). Upon substituting $u_p = u - u_r$ (11) becomes

$$\frac{du_r}{dz} = v_r K \left[1 + \frac{u_r^2}{w_p^2} \right]^{1/2} + \frac{du}{dz}. \quad (14)$$

In its present form (14) is not integrable without applying some conditions. The first of these is that over a sufficiently small layer of integration K is constant and the second is that $u_r^2 \ll w_p^2$.

If, in addition, we examine the particular case in which the vertical wind shear is zero, then

$$\frac{du_r}{dz} = Ku_r; \quad (15)$$

and its solution is

$$u_r(z) = u_r(z_0) \exp[-K(z_0 - z)], \quad (16)$$

where $u_r(z_0)$ is the initial wind error at height z_0 and $z \leq z_0$. Equation (16) demonstrates that the wind error decreases exponentially with the distance the sensor falls through the atmosphere.

Maintaining the same prescribed conditions and letting the vertical wind shear vary sinusoidally, (14) becomes

$$\frac{du_r}{dz} = Ku_r + \frac{2\pi A_m}{L} \sin \left[\frac{2\pi}{L} (z_o - z) \right] \quad (17)$$

where $2\pi A_m/L$ is the amplitude and L its wavelength.

A solution for steady-state conditions is given by Middleton and Spilhaus (1953, p. 66).

$$u_r = - \frac{A_m}{\sqrt{1 + K^2 L^2 / 4\pi^2}} \sin \left[\frac{2\pi}{L} (z_o - z) - \tan^{-1} \frac{2\pi}{KL} \right]. \quad (18)$$

If we substitute $(u - u_p)$ for u_r and denote the phase angle by ψ , we obtain

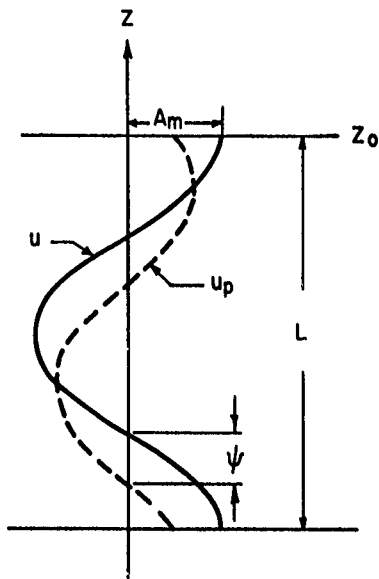
$$u_p = u + \frac{A_m}{\sqrt{1 + K^2 L^2 / 4\pi^2}} \sin \left[\frac{2\pi}{L} (z_o - z) - \psi \right] \quad (19)$$

where $u = A_m \cos \left[\frac{2\pi}{L} (z_o - z) \right]$.

This result shows a wind speed indication of reduced amplitude which lags behind the real wind speed fluctuations in the environment. As expected, increasing values of either K or L increase the amplitude of the wind speed indication and reduce the phase angle. Fig. 2 is a plot of (19).

4. QUANTITATIVE RESPONSE CHARACTERISTICS

In order to investigate quantitatively the response of a wind sensor to its environment, it is necessary to deal with the physical characteristics of the environment and sensor. The remainder of this report will be concerned with the ARCAS parachute.



RESPONSE OF SENSOR SPEED u_p TO OSCILLATORY WIND SPEED u OF AMPLITUDE A_m AND WAVELENGTH L UNDER STEADY-STATE CONDITIONS. ψ IS THE PHASE ANGLE.

FIG. 2.

The parachute is launched aboard an ARCAS rocket, ejected in the vicinity of 80 km and tracked by radar. Figure 3 has been constructed from data contained in a report by the Atlantic Research Corporation (1962). It should be noted that because the ejection time is fixed at 128 seconds, the separation of the sensor from the carrier can (and does) occur before, at, or after apogee (point C). For this reason, and because of yaw and pitch of the rocket, the direction of ejection is uncertain. After ejection, all three components (motor, nose cone, and parachute) are tracked until the parachute becomes the largest radar target. No information is in general made available as regards the "blossoming" of the parachute. Winds are normally calculated beginning at the point where the wind sensor is deemed to be "wind sensitive" (point D, Fig. 3). This point is ascertained subjectively from the radar track by noting a "discontinuity" in the plotted path.

The aerodynamic performance of the falling parachute is dealt with elsewhere (Beyers, et al, 1962; Whitlock and Murrow, 1964). It is sufficient to note that the effective cross-sectional area varies with descent (by virtue of the shroud lines twisting and the pendulum motion induced by the instrument package) and the parachute may slip and glide and perhaps collapse altogether. These effects are more predominant at the higher altitudes. Since we are interested in altitudes from 30 to 80 km, the variation of K with height must be taken into account. We shall first consider the vertical variation of the drag coefficient, C_D .

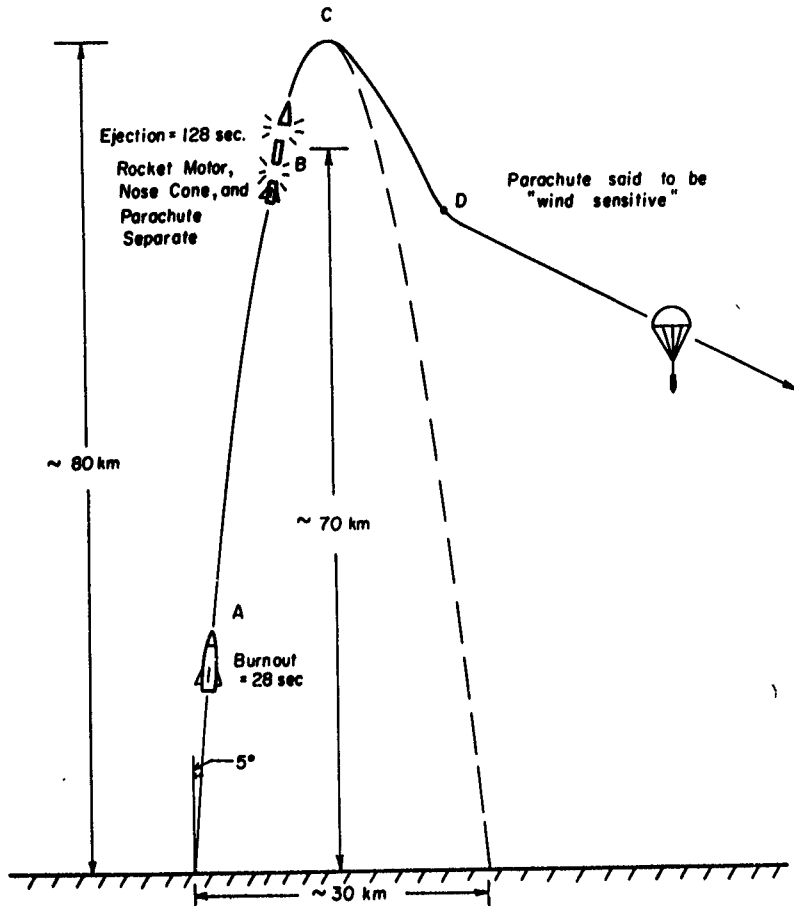
SCHEME OF IDEALIZED *ARCAS* PARACHUTE FLIGHT

FIG. 3.

Wagner (1964) has fitted an analytical curve to an average fall speed profile based on many trials and produced the expression

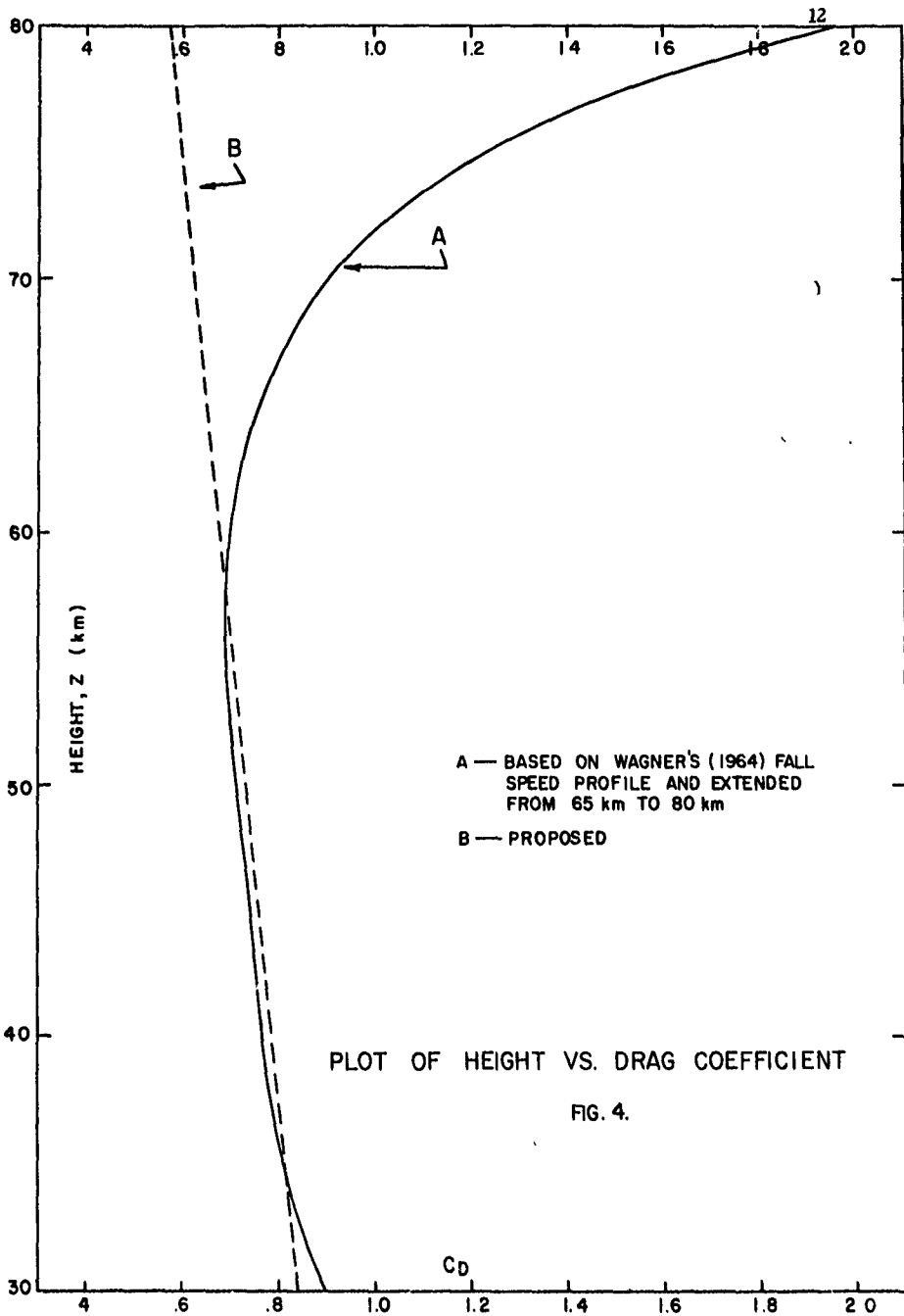
$$w_p = -K_1 \exp[(K_2 z - K_3)^{1/2} - K_4], \quad (20)$$

where the K's are empirical constants. The data from which (20) was deduced, however, were taken from the 30-65 km layer only. The effect of this equation above 65 km can be determined in the first instance by using it to generate a C_D profile.

Let us imagine that we have released the parachute at 80 km into a calm atmosphere. Then u_r and v_r are zero so that (13) can be solved for C_D resulting in

$$C_D = (2m/\rho A) \left[\frac{1}{w_p} \frac{dw_p}{dz} + \frac{g}{w_p^2} \right] \quad (21)$$

The C_D profile has been computed after substituting (20) into (21) for w_p , using the U. S. Standard Atmosphere density (Duberg, et al, 1962), $A = 164045 \text{ cm}^2$, and $m = 2330 \text{ gm}$. In Fig. 4 (curve A) the drag coefficient continually increases above 60 km. We see no apparent justification for this on physical grounds. Rather, the increase is a consequence of extrapolating Wagner's w_p profile to heights where its application was not intended. As (20) indicates, w_p increases without bound as z increases. This, of course, is unrealistic because the fall speed must be zero at apogee.



On the other hand, the C_D profile should be acceptable below 60 km because it is based on empirical w_p data. In order to obtain a plausible C_D profile for the entire 30-80 km region, we shall assume simply that C_D varies linearly with height and is strongly weighted by the data below 60 km.

The expression for the drag coefficient is

$$C_D = 1 - 0.00533z \quad (22)$$

where z is in kilometers. Eq. (22) is also shown in Fig. 4 (curve B).

We now have sufficient information to derive a new w_p profile that will be more consistent with expectations above 60 km. To accomplish this, we need first to integrate (11) and (13). The integration will be performed over a layer 500 m thick in which we shall assume a mean value of K and the two terms u_r and w_p inside the radical (let $v_r = 0$). The results of integrating (11) and (13) are, respectively,

$$u_r = [u_r(z_0) + B^{-1} \overline{du/dz}] \exp[-B(z_0 - z)] - E^{-1} \overline{du/dz} \quad (23)$$

and

$$w_r = \left\{ [w_r^2(z_0) - gB^{-1}] \exp[-2B(z_0 - z)] + gB^{-1} \right\}^{1/2}, \quad (24)$$

where

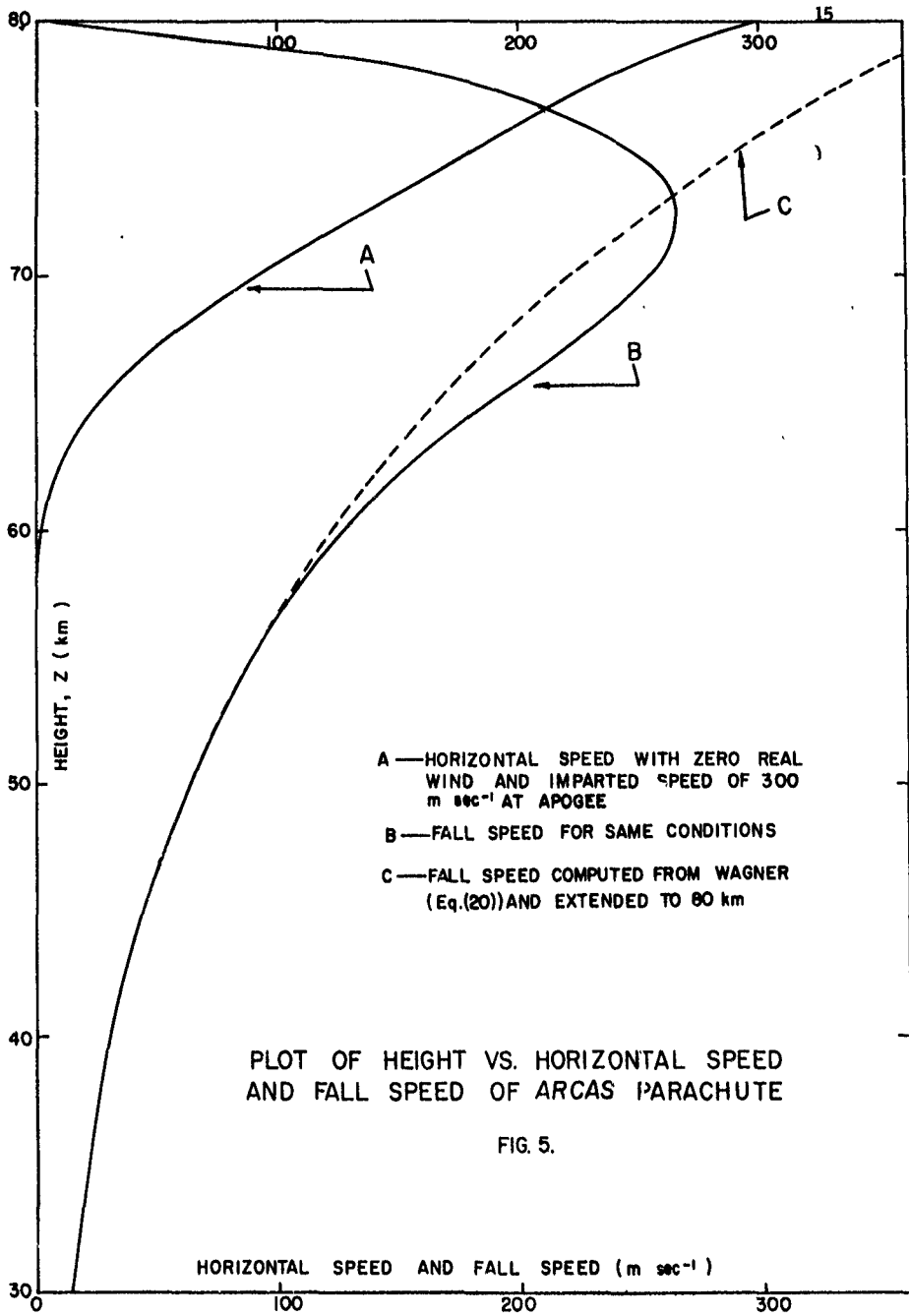
$$B = \overline{K} [1 + (\overline{u_r/w_r})^2]^{1/2}. \quad (25)$$

Equations (23) and (24) have been applied to successive layers 500 m thick commencing at 80 km and proceeding downward to 30 km. The

numerical computational procedure for each layer was begun by computing B from an initial guess of \bar{u}_r and \bar{w}_r . \bar{C}_D was computed from (22) and $\bar{\rho}$ from the Standard Atmospheric density. Given the boundary conditions $u_r(z_0)$ and $w_r(z_0)$, and the mean shear $\overline{du/dz}$, u_r and w_r were computed for the bottom of the layer in question. The values of u_r and w_r were used to obtain new values of \bar{u}_r and \bar{w}_r and, then, an "improved" estimate of B. This value of B was substituted into (23) and (24) to arrive at improved estimates of u_r and w_r . The iterative procedure continued until no significant change in B resulted. The final values of u_r and w_r were used as the upper boundary conditions for the next layer down.

The computed u_r and w_r profiles for zero real wind ($u(z) = 0$) and the boundary conditions $u_r = 300 \text{ m sec}^{-1}$ and $w_r = 0 \text{ m sec}^{-1}$ at 80 km are displayed in Fig. 5 along with Wagner's fall speed profile [Eq. (20)]. A sensor speed of 300 m sec^{-1} imparted by the rocket at apogee is not unrealistic. The similarity of the two fall speed profiles below 60 km is a direct consequence of utilizing nearly the same drag coefficient in (24) as that predicted from Wagner's fall speed equation and there being practically zero wind error. Their diversity above 60 km follows from opposite reasons. Additionally, Fig. 5 shows that the parachute must fall 20 km to a height of 60 km before the wind error is negligible.

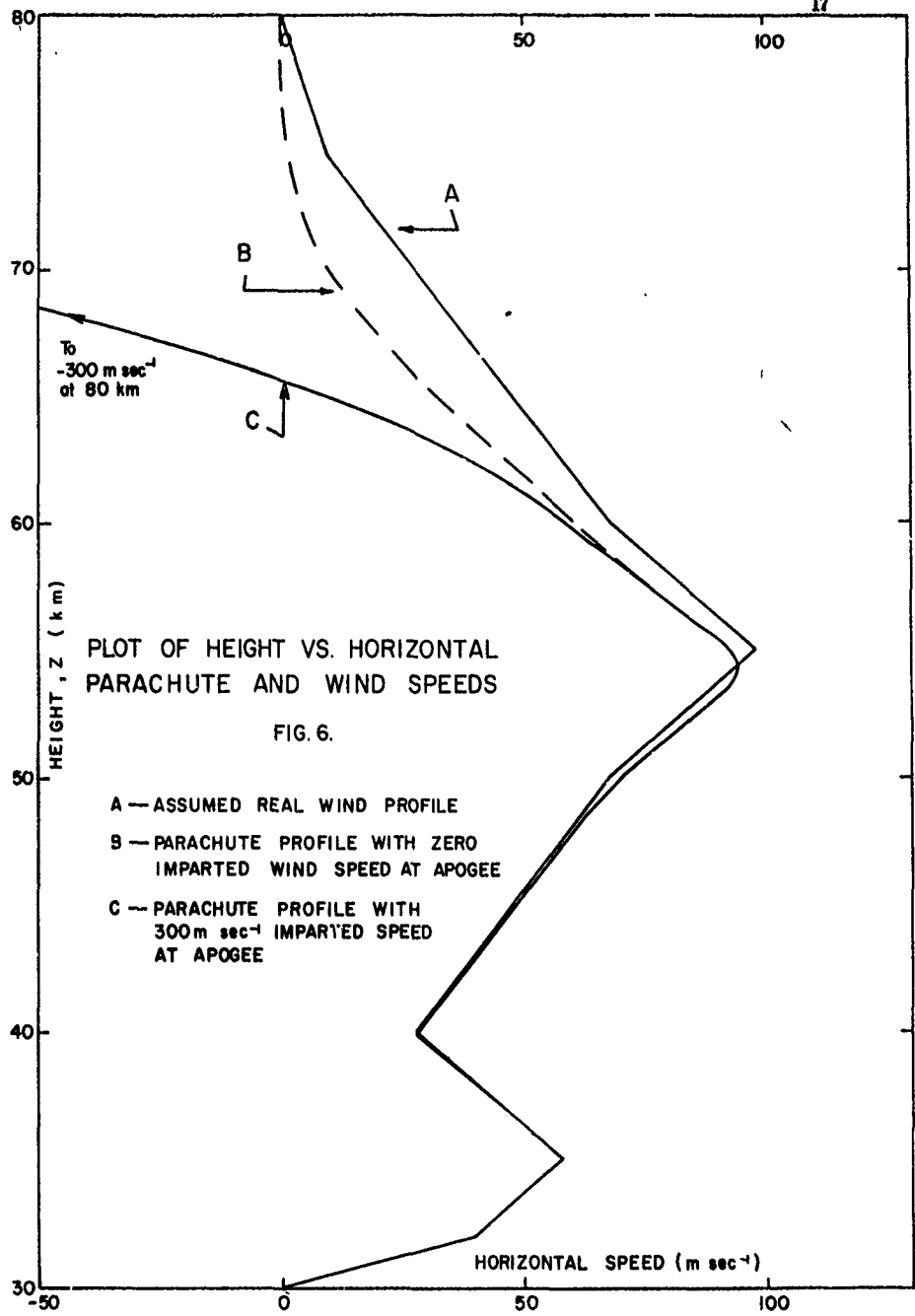
As seen in (24) and (25) the fall speed is dependent on the wind error u_r . The significance of this dependence can be examined by postulating another real wind profile with different boundary conditions on u_r at apogee

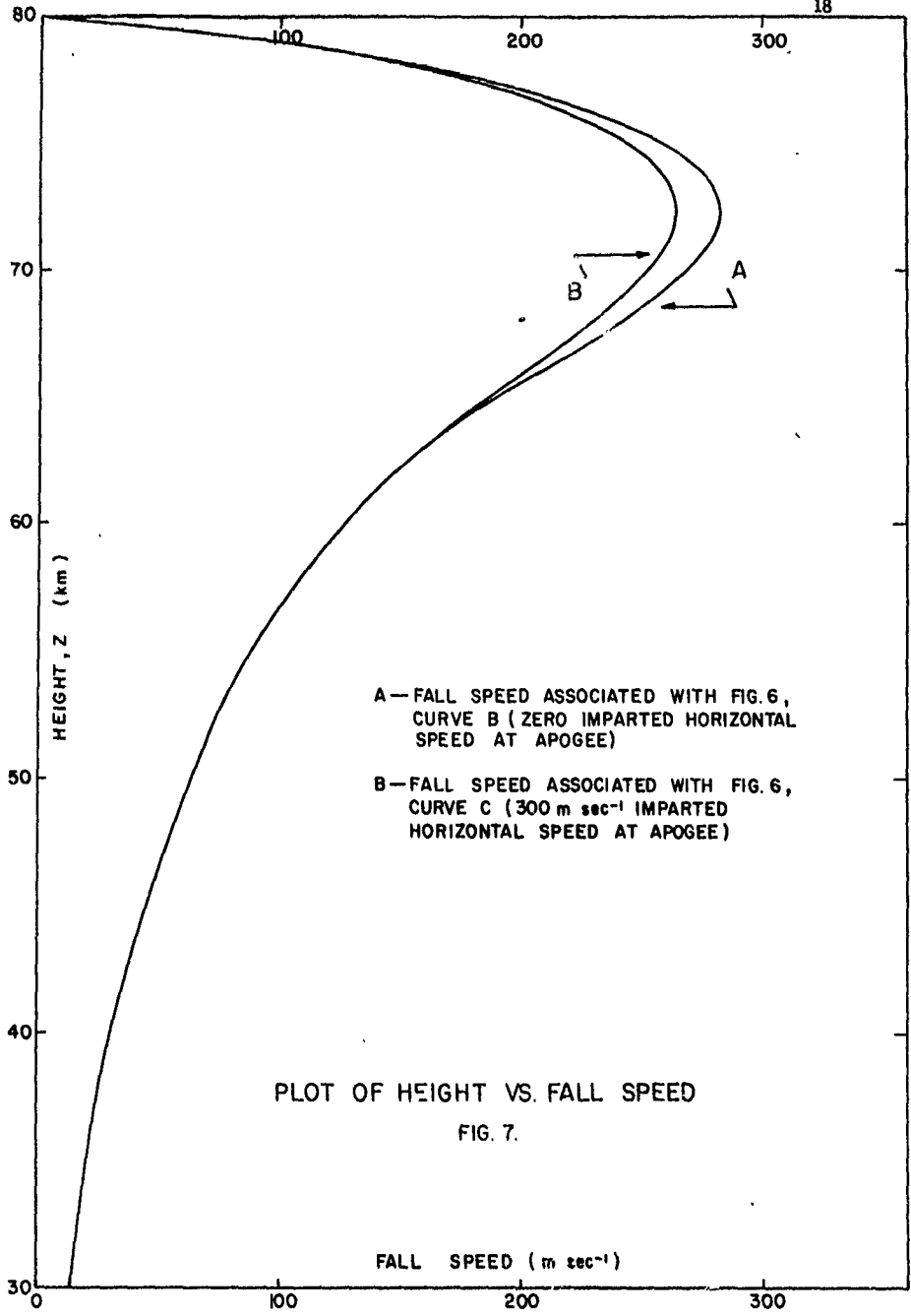


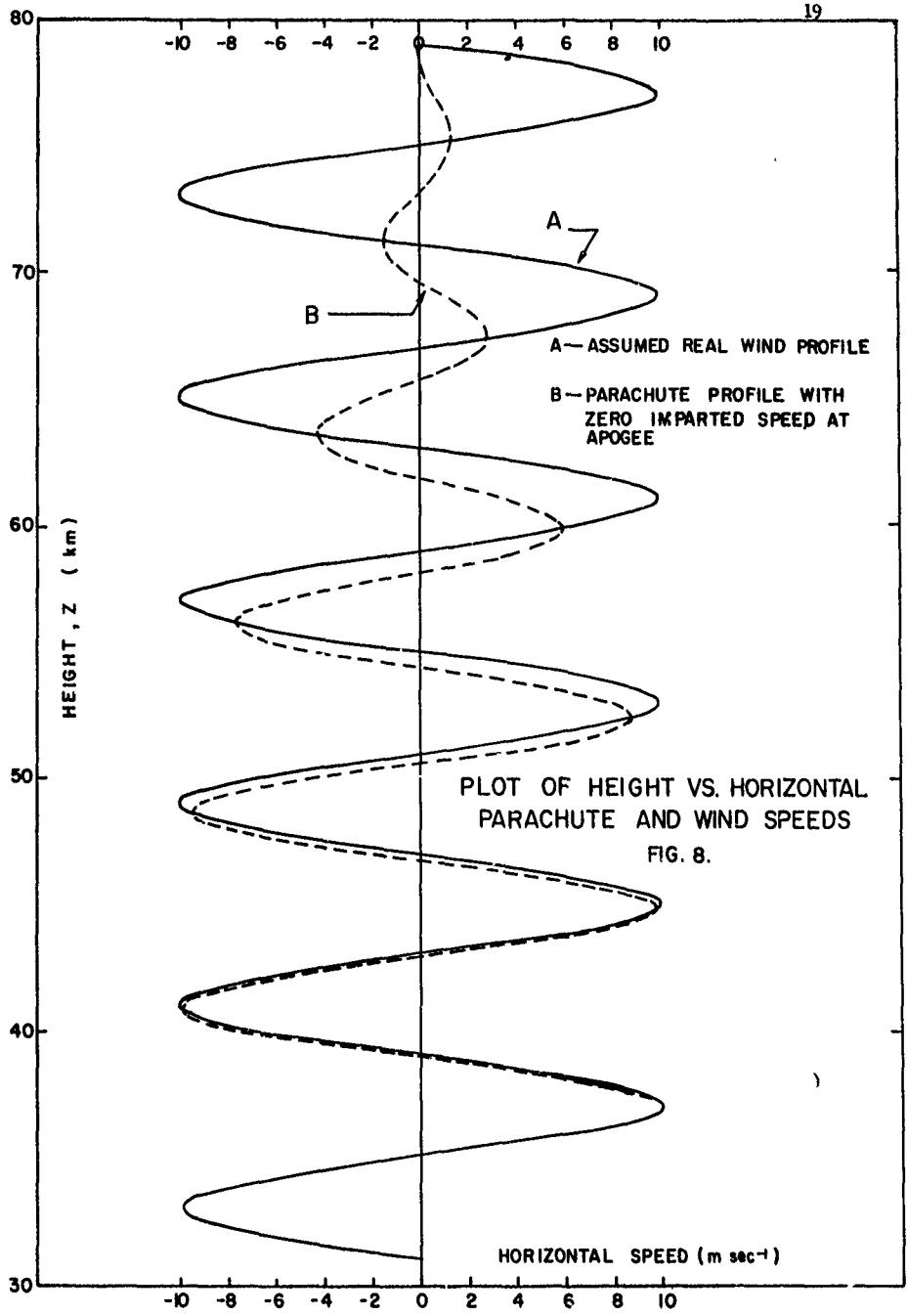
and comparing the computed w_r or w_p profile with that in Fig. 5 (curve B). The assumed real wind profile is shown in Fig. 6 (curve A).

The u_r and w_r profiles were computed in the manner previously prescribed. The differences between the u_p profiles shown in Fig. 6 and between the w_r (or w_p) profiles shown in Fig. 7 are the result of making $u_r = 0$ at apogee in one case and $u_r = 300 \text{ m sec}^{-1}$ in the other. Figure 6 illustrates, as did Figure 5, that the effect on the speed of the sensor of the impulse imparted to it by the rocket is almost negligible at 60 km. In Figure 7 we observe that despite the 300 m sec^{-1} difference in horizontal speed at apogee, there is only a small difference in the fall speed profiles. The maximum difference of about 7% occurs near 72 km. A comparison of curves B in Figs. 7 and 5 ($u_r(80) = 300 \text{ m sec}^{-1}$) indicates they are nearly the same; the maximum difference is about 1%. The conclusion ensues that the effect of the ratio u_r^2/w_r^2 on the fall speed is slight and can be neglected.

We now consider one additional hypothetical case in which we have an 8 km vertical wave in the u-profile. The aforementioned iteration procedure among (23), (24), and (25) produces the results shown in Fig. 8. The wind error at the top of the profile was assumed to be zero. The parachute fall speed profile has not been shown since it is virtually identical with that in Fig. 7 (curve A). Figure 8 reveals that even after falling to a height of 60 km the phase shift is 45° and the observed amplitude is only 60% of the wind amplitude. The sensor must fall an additional 20 km before it is almost completely responsive to the wind. Of course, as the wavelength decreases, the response of the parachute also decreases.







PLOT OF HEIGHT VS. HORIZONTAL PARACHUTE AND WIND SPEEDS

FIG. 8.

Figures 9 and 10 display, respectively, the response and phase angle dependence on both wavelength and height. In Fig. 9 we have plotted the response, i. e., the ratio of the observed amplitude to the wind amplitude, as a function of wavelength at various heights. The ratio of the respective amplitudes, as determined from Eq. (19), is $1/[1 + (4\pi^2/K^2 L^2)]^{1/2}$. At any given wavelength, the response increases with decreasing altitude. At 8 km only 10% of the amplitude of the longest wavelength (16 km) is detected whereas at 30 km more than 99% of the amplitude of all wavelengths greater than 1 km is detected by the parachute.

In Fig. 10 we see that at any given height the phase angle decreases with increasing wavelength. At 80 km the phase shift is greater than 80° for all wavelengths shown whereas at 30 km the phase shift is less than 5° for all wavelengths.

5. APPLICATION TO REAL WIND DATA

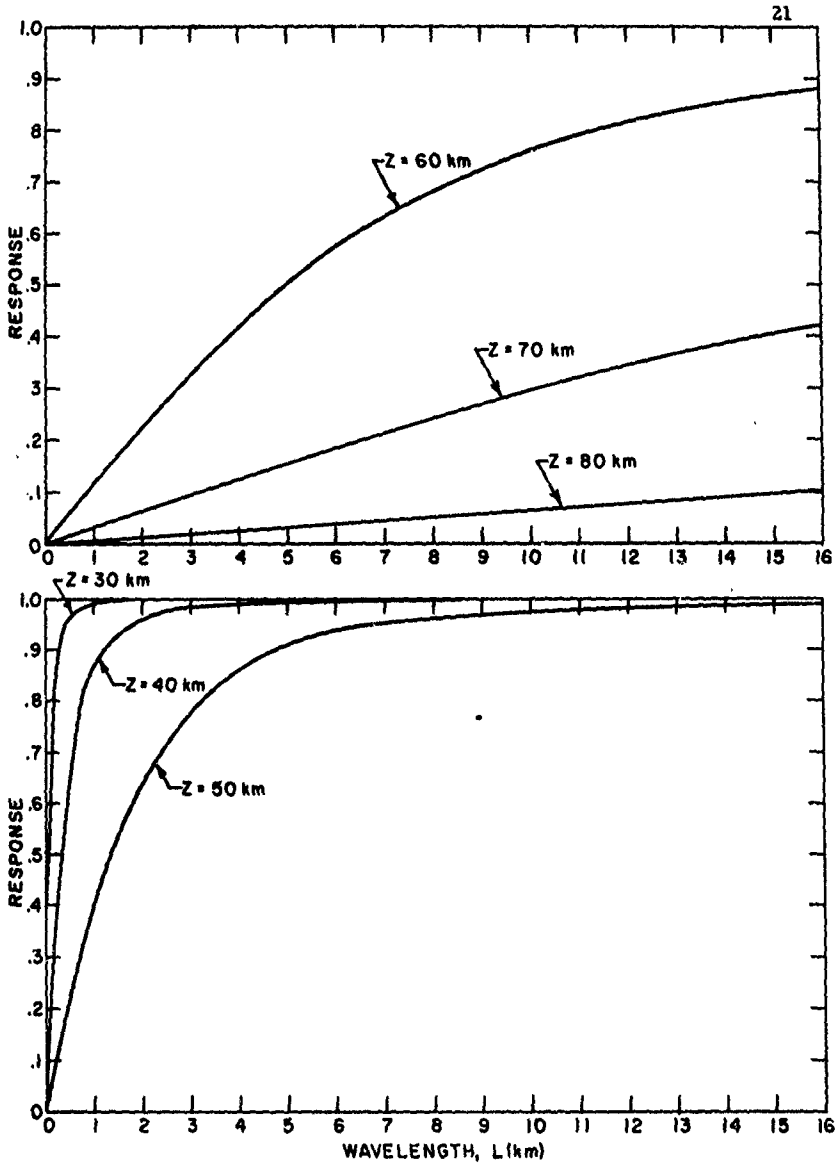
As pointed out in Section 2, if we assume no vertical wind, we can deduce the wind structure from the observed motion of the falling parachute; that is, by substituting (7) into (5) and (6), we obtain

$$u = u_p - (w_p \frac{du_p}{dt}) / [\frac{dw_p}{dt} + g], \quad (26)$$

and

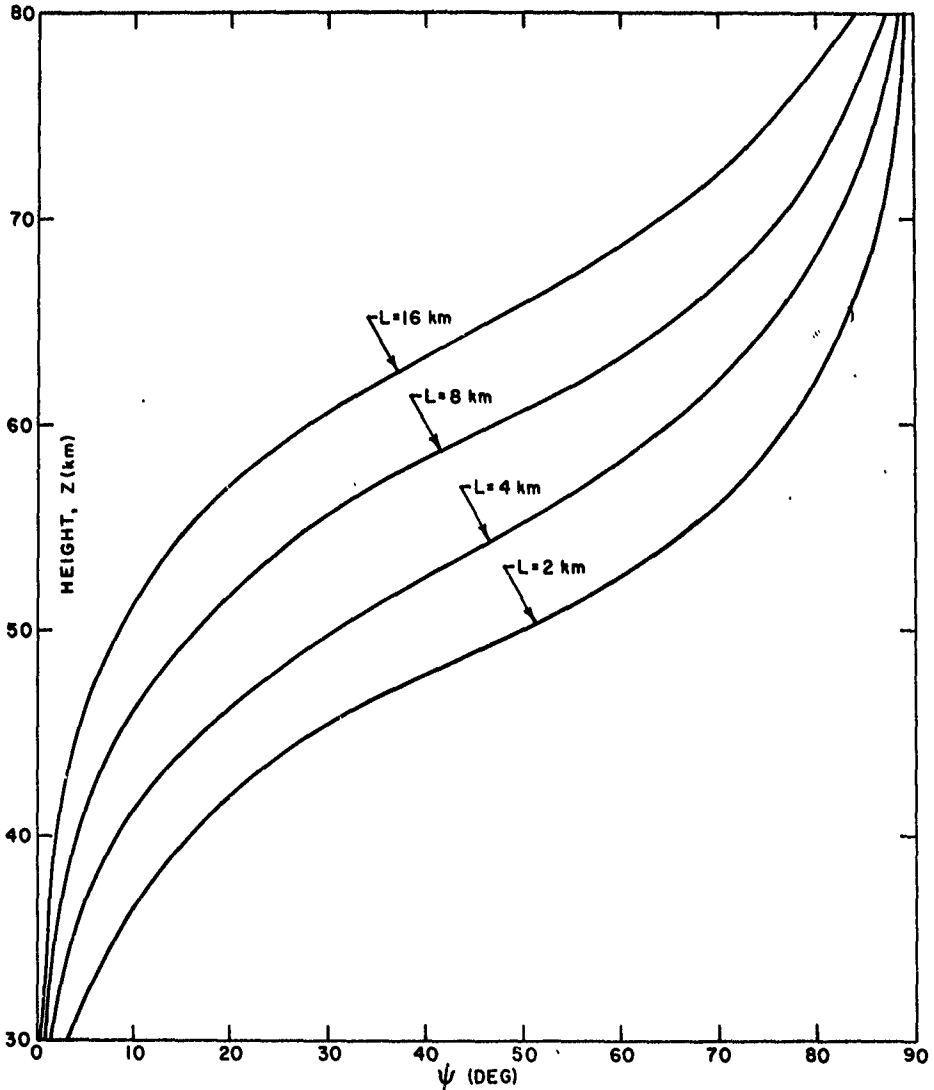
$$v = v_p - (w_p \frac{dv_p}{dt}) / [\frac{dw_p}{dt} + g]. \quad (27)$$

We shall apply (26) and (27) in finite-difference form to an actual



FREQUENCY RESPONSE OF *ARCAS* PARACHUTE vs
WAVELENGTH AT VARIOUS HEIGHTS

FIG. 9



HEIGHT vs PHASE ANGLE $\psi = \tan^{-1} \frac{2\pi}{KL}$ FOR
VARIOUS WAVELENGTHS

FIG. 10

sounding from the ARCAS parachute. The data (parachute position, velocity, and acceleration) are contained on magnetic tape and have had a 101-point filter applied to the various parameters (Webster, 1964). The frequency response of this filter can be deduced from the numerical operator employed; however, let it suffice here to say that the smoothing effected is very little, indeed, even at the high frequency end of the spectrum. Equation (26) can be written in finite difference form as

$$u(i) = u_p(i) - \left[w_p(i) \frac{u_p(i+1) - u_p(i-1)}{2\Delta t} \right] / \left[\frac{w_p(i+1) - w_p(i-1)}{2\Delta t} + g \right], \quad (28)$$

where i denotes the current value, $i-1$ the previous value, and $i+1$ the subsequent value. $\Delta t = 0.1$ second and $g = 32.174 \text{ ft/sec}^2$. An analogous relation holds for the v -component (Eq. (27)).

Because the sensor falls at a variable speed (about 4 times as fast at 60 km as at 40 km) and the data are spaced in equal time increments, a symmetrical filter applied to the data is automatically a function of height.

A second 101-point symmetrical filter has been designed to eliminate certain undesired waves in the data. The theoretical (continuous) frequency response of this filter is given by:

$$R'(f) = \exp(-16f)^2 \quad (29)$$

where f is in cycles per second. The corresponding weight function providing this response is

$$w(t) = (\pi^{1/2} / 16) \exp(-\pi t / 16)^2, \quad (30)$$

when t is in seconds.

The response to a discrete 101-point symmetrical filter is given by

$$R(f) = W(0) + 2 \sum_{j=1}^{50} W(j) \cos(2\pi j f), \quad (31)$$

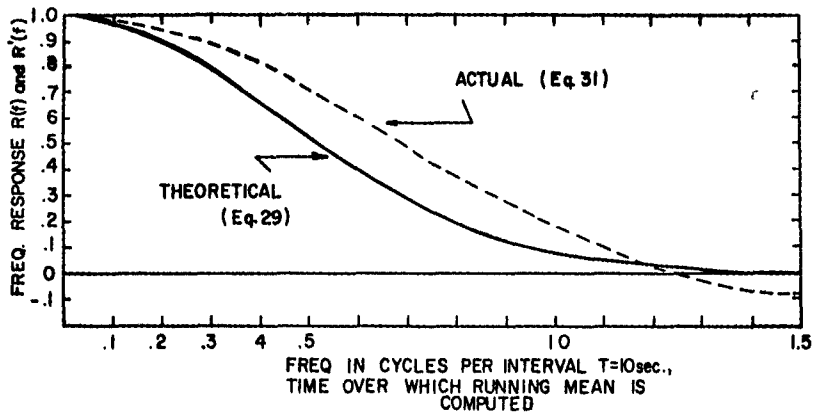
where the $W(j)$ are determined from (30) subject to the constraint*

$$W(0) + 2 \sum_{j=1}^{50} W(j) = 1.$$

Equations (29) and (31) are plotted in Fig. 11. Fig. 12 displays the response as a function of wavelength at various heights assuming the fall speed profile in Fig. 7 (curve B). We note that for waves in u_p and v_p less than 125 m in wavelength, less than 10% of their amplitude is retained at 30 km, whereas at 70 km the same percentage applies to wavelengths less than 2250 m.

The results of applying (28) and its counterpart to the smoothed u_p , v_p , and w_p data for the flight under consideration are shown in Fig. 13. Below about 58 km the difference between the associated horizontal components of the parachute and wind speed are small. Above this level the differences increase to a height of about 72 km. From this point to apogee (75 km) the computed wind speed components are very erratic. Not all the computed wind speed components are plotted for this region because their magnitude was off the scale of the graph.

* For further information on filtering techniques refer to Holloway (1958).



FREQUENCY RESPONSE FUNCTIONS

FIG. 11

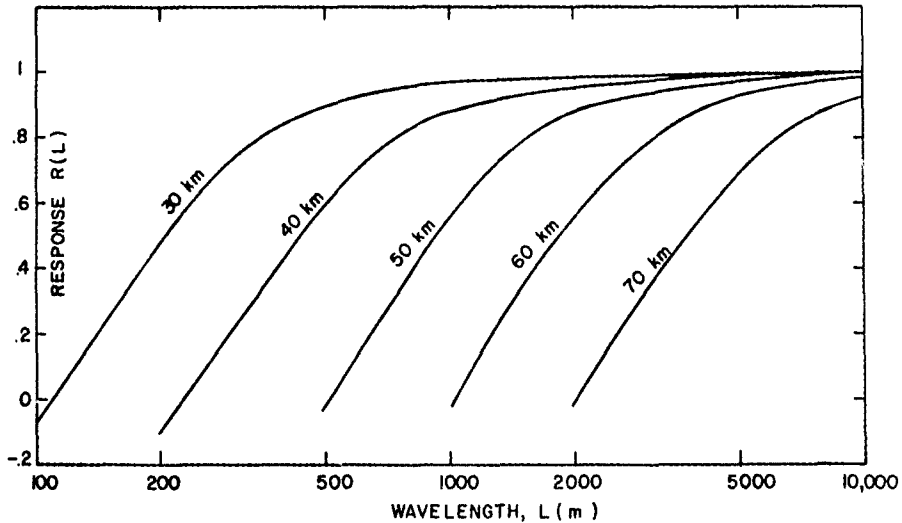
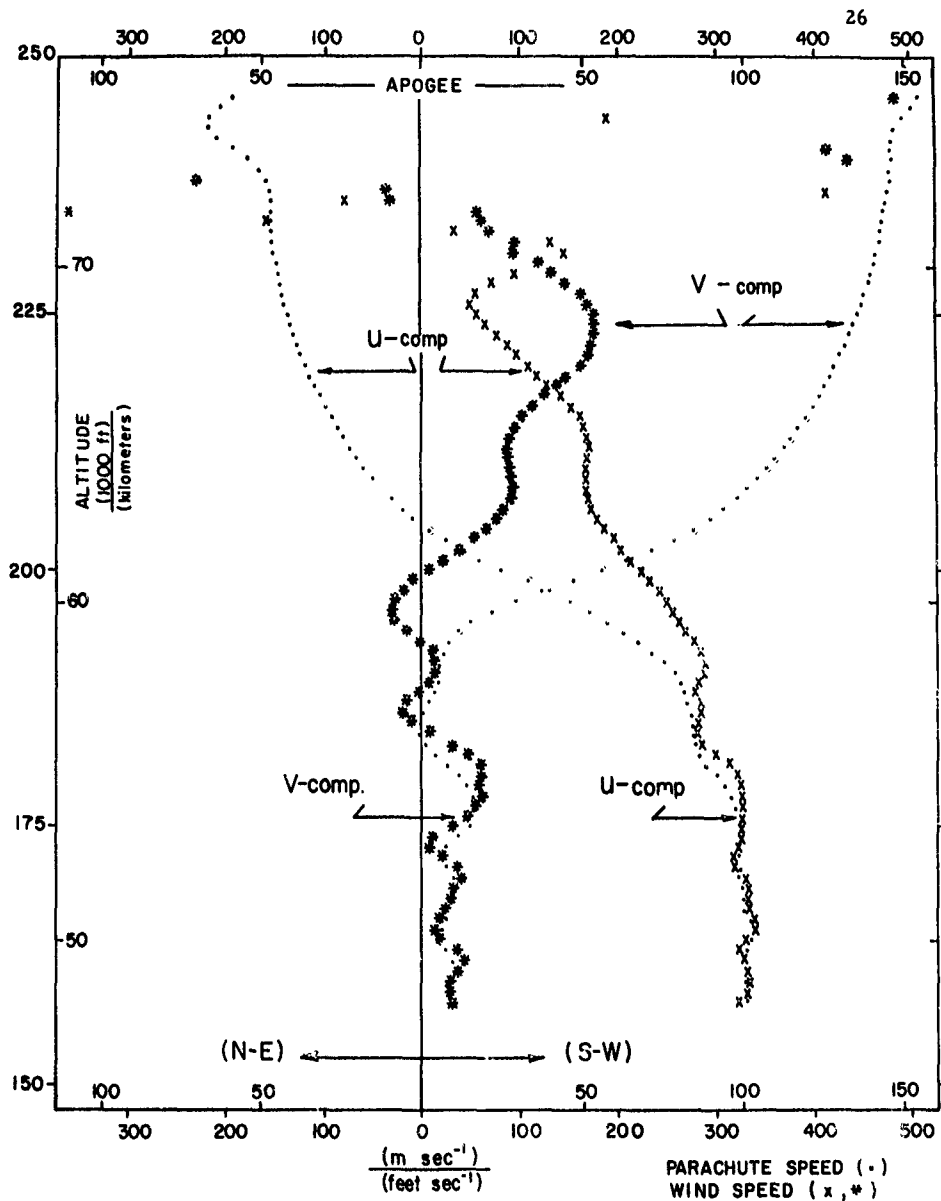
RESPONSE AS A FUNCTION OF WAVELENGTH FOR
VARIOUS HEIGHTS

FIG. 12



COMPUTED WIND SPEEDS FROM OBSERVED
PARACHUTE SPEEDS

FIG. 13

An examination of the vertical accelerations of the parachute in the latter region reveal that they fluctuate rapidly in time from values less than g to values greater than g ; in one instance from 15 ft sec^{-2} to 45 ft sec^{-2} in one second. As seen in Eqs. (26) and (27), when the vertical acceleration of the parachute approaches g the correction term approaches infinity. Whether these accelerations are real or are a consequence of the inability of the radar to correctly track the parachute is not known. If the accelerations are real then it may be that there are other forces present that have not been accounted for in Eq. (1).

The response features exhibited in Fig. 13 are consistent with those described in the previous two sections of this report, at least up to about 68 km. It is quite apparent that large corrections must be applied to the measured winds above 60 km in order to obtain the true winds. In the example considered, the corrections varied from about 40 m sec^{-1} to about 100 m sec^{-1} in the 60-70 km region.

6. SUMMARY

This report has dealt with the response of a wind sensor acting only under the influence of aerodynamic drag and gravity. The following assumptions were made: zero vertical wind, the physical characteristics of the sensor and environment constant with height, and the ratio of the wind error (difference between the horizontal wind and parachute speeds) to the fall speed small compared to unity. Under these conditions, it was found that the equation for the response of the wind sensor was of the same form

as that for the response of an ordinary mercury thermometer.

Next, the equations of motion (assuming zero vertical wind) were applied to the ARCAS parachute. The Standard Atmosphere density and a semi-empirical drag coefficient profile were employed for the 30 to 80 km region. By postulating various wind profiles for this layer and different ejection speeds at apogee (80 km) the following results were established:

1. in cases of zero to moderate horizontal wind shear, the parachute must fall from 80 km to approximately 60 km before it becomes essentially "wind sensitive" (wind error on the order of a few meters per second);
2. the parachute fall speed profiles are all approximately the same;
3. the effect of the ratio of the wind error to the fall speed on the fall speed is small.

Last, and most significant, a simple numerical procedure was developed from the equations of motion (assuming zero vertical wind) that can be used to compute the wind structure from the observed sensor motion. This procedure involves neither the physical characteristics of the sensor nor those of the environment. Of additional significance is the fact that this procedure does not depend on the power of the velocity term in the equation for the drag force.

This technique was applied to an actual ARCAS flight and the computed component wind speed corrections were as large as 100 m sec^{-1} in the 60-70 km region.

REFERENCES

- Atlantic Research Corporation, 1962: ARCAS rocket system training manual. Atlantic Research Corporation, Alexandria, Virginia.
- Beyers, Norman J., Otto W. Thiele, and Norman K. Wagner, 1962: Performance characteristics of meteorological rocket wind and temperature sensors. Tech. Rept. SELWS-M-4, Missile Meteorology Division, USAERDA, White Sands Missile Range, New Mexico, 29 pp.
- Duberg, John E., et al., 1962: U. S. Standard Atmosphere 1962. Government Printing Office, Washington, D. C., 278 pp.
- Holloway, J. L., 1958: Smoothing and filtering of time series and space fields, in Advances in Geophysics, Vol. 4, 351-389, Academic Press, Inc., New York, 456 pp.
- Middleton, W. E. K., and A. F. Spilhaus, 1953: Meteorological Instruments. University of Toronto Press, 286 pp.
- Wagner, Norman K., 1964: Theoretical accuracy of a meteorological rocketsonde thermistor. J. Appl. Meteor., 3, 461-469.
- Webster, E., 1964: Velocity and acceleration program (v and a) for IBM 7094 computer, revision I. Programming Section, Computing Branch, Data Reduction Division, White Sands Missile Range, New Mexico, 42 pp.
- Whitlock, C. H., and H. N. Murrow, 1964: Performance characteristics of a preformed elliptical parachute at altitudes between 200,000 and 100,000 feet obtained by in-flight photography. NASA Tech. Note D-2183, Langley Research Center, Langley Station, Hampton, Virginia.